

Effect of Electrolyte Concentration and Depth of Discharge for Zinc-Air Fuel Cell

Guanghua Li, Ke Zhang, Mohammed Adnan Mezaal, Rui Zhang, Lixu Lei*

School of Chemistry and Chemical Engineering, Southeast University, Nanjing 211189, China

*E-mail: lixu.lei@seu.edu.cn

Received: 19 April 2015 / Accepted: 20 May 2015 / Published: 24 June 2015

To understand the origins of performance variations in zinc-air fuel cell (ZAFC), the experimental study on the effects of the ZAFC for electrolyte concentration and depth of discharge was carried out by voltammetric, discharge profile and EIS methods. The highest cell performance was achieved at 7 M KOH, which resulted in a maximum current density of 102.0 mA cm^{-2} at 1.0 V vs. Zn. Moreover, R decreased in high-frequency when the discharge time increased, it is related to total ohmic resistance in the ZAFC. The degradation of ZAFC increases with increasing discharge time. The observed trend is favorable for confirming the time of replacing the zinc plate and (or) the electrolyte in ZAFC.

Keywords: Oxygen reduction reaction; Zinc oxide; Zinc-air fuel cell; Polarization curve

1. INTRODUCTION

Various types of zinc-air batteries (ZABs) and fuel cell (ZAFC) have been researched because of their high specific energy, low-level pollution, and low operation risks, for example primary battery, rechargeable battery and fuel cell [1, 2]. Zinc-air primary battery has already commercialized in hearing aids, mobile applications, navigation lights, and railway signals so forth, however, that is not applicable to electric vehicles (EVs) [3-5]. Moreover, the problem of cyclife limits the electrically rechargeable battery applied to the fields of transportation and energy storage [6]. In ZAFC, zinc metal as an anode material is abundantly available, inexpensive, non-toxic, safe, and easy to handle and store [7]. Air is an oxygen source to be supplied at the cathode side, while aqueous alkaline solution is an electrolyte. It works on the basis of a reaction between the O_2 and Zn plate in alkaline condition [8]. The advantages of ZAFC are using inexpensive materials of catalysts and separators, the high energy density, stable discharge voltage and running at ambient temperature. The ZAFC has huge potential as an alternative energy generator for EVs, because the produces only ZnO , which is absolutely

recyclable, without gas emission while generating electricity [9]. If successfully developed, it could enable EVs with driving ranges similar to those of gasoline-powered vehicles [10].

Recently, in order to improve the zinc-air system, a mass of work to be addressed. Wu *et al.* prepared solid PVA/PAA polymer electrolyte membranes for use in alkaline zinc-air and aluminum-air cells [11]. The experimental study on the improvement of ZAFC performance was carried out for flowing electrolyte with and without gelling agent [12]. Chao *et al.* prepared catalytic layer of air electrode by the clay to dispersant to improve the ZAFCs performance [13]. The use of tapioca binder for zinc anode can improve the discharge specific capacity in ZABs [14]. Cho *et al.* reported that surface treatment of zinc anode to improve discharge capacity and suppress hydrogen gas evolution in ZABs [15]. MCM-41 as a new separator material for ZABs was used [16]. Coating on zinc surface with nickel to improve the electrochemical behavior of zinc anode for ZAFCs [17]. The use of calcium hydroxide for scavenging zincate species is demonstrated to be a highly effective approach for increasing the electrolyte capacity and improving the performance of the ZAFC system [18]. However, the ZAFC is yet in initial stage of commercialization due to have any uncertainties for which further research need to be reported.

In this work, the influence of the ZAFC performance was continued to be investigated. To thoroughly understand the nature of ZAFC, we have made detailed effects of zinc electrode and electrolyte concentrations. The effects of the ZAFC for electrolyte concentration and depth of discharge was carried out by voltammetric, discharge profile and EIS methods. Moreover, zinc oxide (ZnO) was synthesized by ZAFC instead of the traditional synthesis approach for example, hydrothermal method, sol-gel, vapour-liquid-solid (VLS) technique, chemical vapor deposition (CVD), and electrochemical deposition [19].

2. EXPERIMENTAL

2.1 Preparation of air electrode and assembly of ZAFC single cell

The air electrode consisted of a gas diffusion layer, a Ni-mesh current collector and an active layer. To prepare the active layer, a mixture containing MnO_2 (EMD) catalyst and acetylene black was grinded for 0.5 h, then the mixture and PTFE suspension (60 wt% in H_2O) with weight ratios of 8:2 were first mixed and ground in excess ethanol and then dried at 80 °C to give a dough-like paste, which was finally rolled into an Ni-mesh of 1.8 mm thickness. To prevent moisture from penetrating from the outside and flooding out the electrolyte from the inside, we attached a waterproof diffusion layer (PTFE membrane, only 0.1 mm thick) to the other side of the active layer as a gas diffusion layer.

A home-made zinc-air fuel cell device was designed for the battery test. The electrolyte used in ZAFC was KOH aqueous solution (4 ml), and a polished zinc plate ($\delta = 0.3$ mm, 3×3 cm 2) was used as the anode.

2.2 Physical characterization and performance measurements

To image the morphologies of the material, scanning electron microscopy (SEM) micrographs of the surface was performed by Hitachi S-4800. X-ray diffraction (XRD) measurements were taken using an X-ray diffractometer (Bruker D8 GADDS) with Cu K α ($\lambda = 0.15406$ nm).

The single cell performance was clearly demonstrated from voltammetric (LSV, at 1 mV s $^{-1}$, from 0.8 ~ 1.5 V vs. Zn), discharge profile and electrochemical impedance spectroscopy (EIS, frequency range: 10 kHz ~ 0.1 Hz, amplitude: 10 mV) analyses. An electrochemical workstation system (CorrTest CS350) and a multichannel battery cycling unit (SZLAND CT2001C) were utilized to perform the measurements at room temperature under air.

3. RESULTS AND DISCUSSION

3.1 Characterization of ZAFCs for pre- and post-discharge

Fig. 1 shows the polarization curves and impedance spectra of ZAFCs with different conditions. Fig. 1a, variations of cell performances with different conditions in fuel cell mode are presented. The difference polarization current densities measured at the same potential of ZAFC (see table 1). The current density of pre-discharge is 101.9 mA cm $^{-2}$, however, which decreased to 6.9 mA cm $^{-2}$ for post-discharge (6.8% for pre-discharge). The performance back to original 47.4%, 62.3%, and 72.9% after renew zinc plate, electrolyte, and zinc plate and electrolyte, respectively. These results indicate that the effects of ZAFCs about electrolyte and zinc anode.

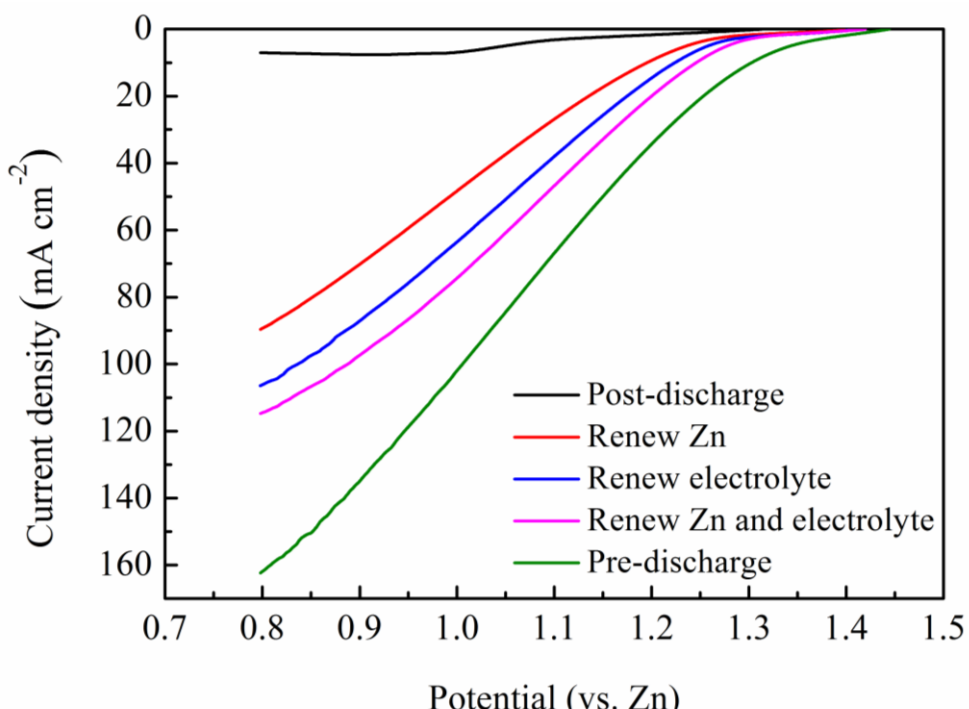
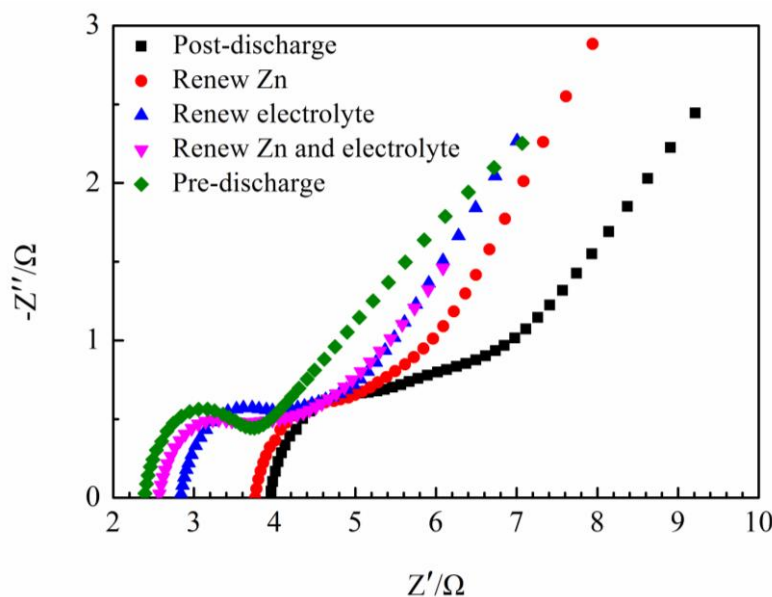


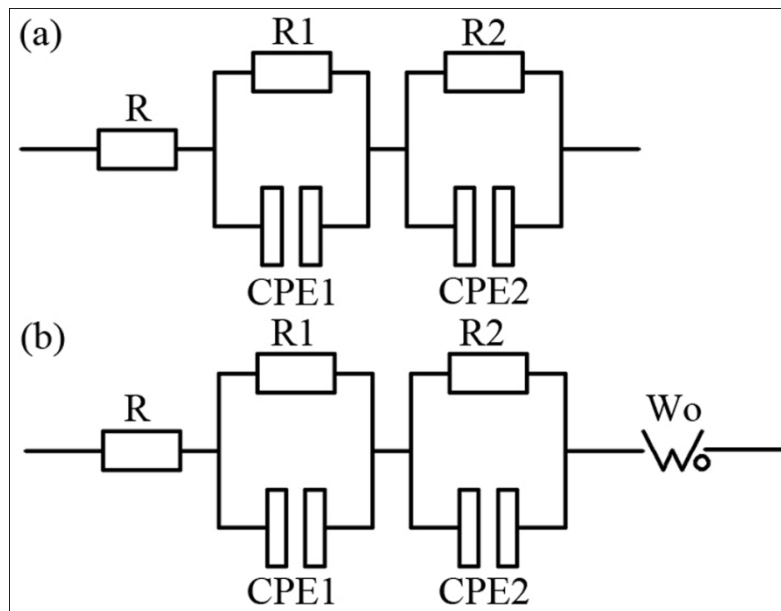
Figure 1. Polarization curves of ZAFCs with different conditions

Table 1. Performances of ZAFCs with difference conditions

	Post-discharge	Renew Zn	Renew electrolyte	Renew Zn and electrolyte	Pre-discharge
Current density at 1.0 V vs. Zn (mA cm^{-2})	6.9	48.3	63.5	74.3	101.9

Fig. 2 shows the impedance spectra of ZAFCs with different conditions at the OCV. Effects of ZAFC about pre- (Fig. 3a), post-discharge (Fig. 3b), renew zinc plate or (and) electrolyte are quantitatively evaluated by the EIS analysis through establishing and fitting a reliable equivalent circuit model (in Fig. 3). The intercept of the impedance spectra at high frequency with the real axis is denoted R, representing the internal resistance of the ZAFC including total ohmic resistance which can be explained as a sum of the contributions arise from uncompensated contact resistance and ohmic resistance of the cell components, for example air electrode, membrane, zinc sheet and that between each of them [20]. R1 is denoted through extrapolation of the onset of the semicircle to the real axis. R1 is the ohmic drop resistance of electrolyte conductivity which depends on air electrode [21]. R2 is denoted the intercept of the impedance spectra at low frequency with the real axis, and R2 is related to the oxygen reduction kinetics (mass-transfer process) [22, 23]. CPE1 and CPE2 are so-called constant phase elements, representing the double-layer [24]. The diffusion element in relatively low-frequency is denoted Wo [25]. As can be seen in Table 2, R increases after discharged, and decreases with renew zinc plate and (or) electrolyte which was expected because R represents the Ohmic resistances of the ZAFCs. Similar trend is observed in R1. R2 has no regularity, so need further research of correlation between of ZAFC performance and the resistance (R2).

**Figure 2.** Impedance spectra of ZAFCs with different conditions

**Figure 3.** The equivalent-circuit model of ZAFCs**Table 2.** Fitted partial data of equivalent circuit parameters about impedance spectra of ZAFCs with difference conditions

	Post-discharge	Renew Zn	Renew electrolyte	Renew Zn and electrolyte	Pre-discharge
R	3.96	3.76	2.84	2.57	2.39
R1	1.78	1.54	1.40	1.32	1.02
R2	1.11	0.78	0.96	0.49	17.25

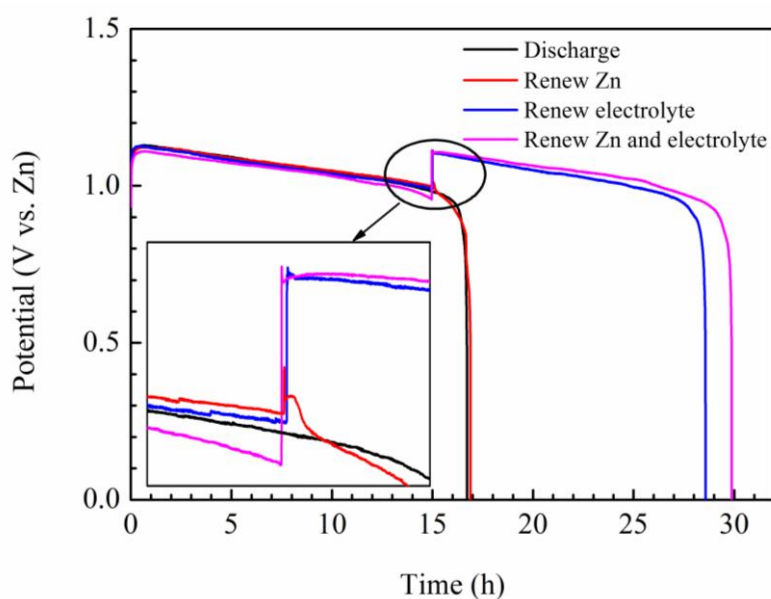
**Figure 4.** Discharge curves for ZAFCs at a constant current density of 50 mA cm^{-2}

Fig. 4 shows discharge curves of ZAFCs at a constant current density of 50 mA cm^{-2} , the open circuit potential all reached $\sim 0.95 \text{ V}$, the average working voltage plateaus all was about 1.0 V . We can see that first curve discharge lasted $\sim 16.5 \text{ h}$. To observe preferably cell performance of change conditions, we choose 15^{th} h as a node. The peak in cell potential at 15 h of operation is caused by instantaneous zero current [26]. When renew a zinc plate at node, no obvious increase of discharge time was observed. However, when renew electrolyte, discharge time increased 12 h . At the same time renew zinc plate and electrolyte, discharge time increased 13 h . These results indicate that the cell performance in agreement with that of polarization curves and impedance spectra. The zinc plate and electrolyte have effects counter ZAFC, and larger influence on the latter.

Fig. 5 shows XRD patterns of ZnO. The sample synthesized using ZAFC, the observed peaks matched quite well with JCPDS no. 05-0664 for ZnO at $2\theta = 31.8^\circ$ (100), 34.4° (002), 36.2° (101), 47.5° (102), 56.6° (110), 62.9° (103) and 67.9° (112). The XRD measurement show that the hexagonal structured ZnO belongs to space group $P6_3/mc$ (186) with lattice parameters of $a = 3.249 \text{ \AA}$ and constant $c = 5.205 \text{ \AA}$. This explains the ZnO of hexagonal nanorod structure observed in SEM images (see Fig. 6).

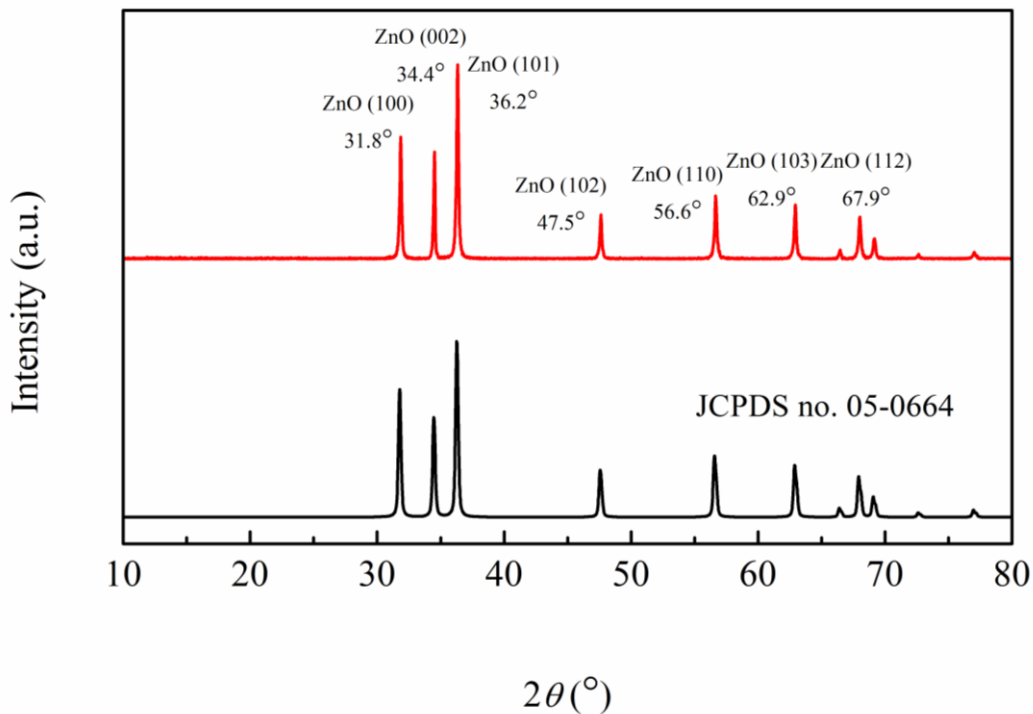


Figure 5. XRD patterns of the ZnO

Fig. 6 shows SEM images of ZnO nanorods synthesized using ZAFC. The nanorods show not of uniform lengths and diameters. It can be observed from this figure that the lengths of the nanorods were $400 \text{ nm} \sim 1 \mu\text{m}$ with diameters of $20 \sim 100 \text{ nm}$.

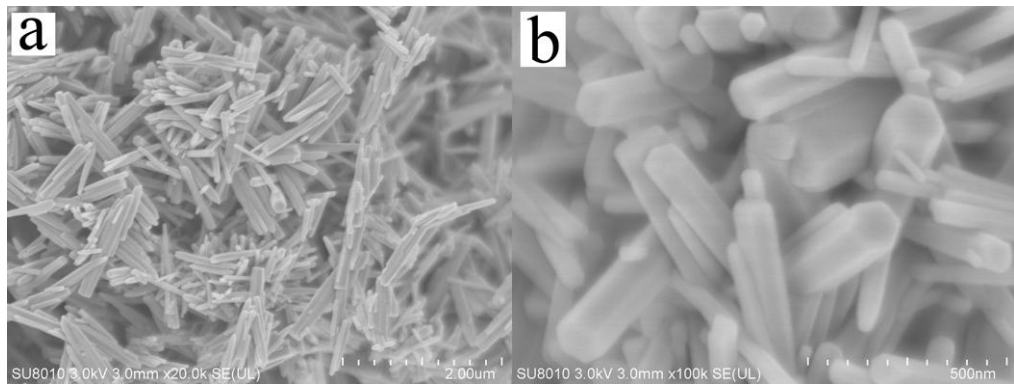


Figure 6. SEM images of ZnO (a), (b) amplification of the (a).

3.2 Effect of the electrolyte concentration for ZAFCs

Fig. 7 shows polarization curves of ZAFC operated in different KOH electrolyte. As can be seen in Table 3, improved ZAFC property is evident with increasing KOH concentrations from 1 to 7 M and achieves the optimal property at 7 M. The observed trend is due to increasing ionic conductivity of the electrolyte, and increasing KOH concentration is contribute to the anode reaction conform to the Nernst equation [27]. However, a further increase in KOH concentrations from 7 to 13 M results in an apparent decrease in ZAFC property. It is due to an increasing the solution viscosity and a decreasing the mobility of ions in KOH solution. In Fig. 7 (or Table 3), using 7 M KOH, which was optimum for the ZAFC. Cao *et al.* reported that the reduction currents increase firstly with KOH concentration before reaching to the maximum values at 2 ~ 4 M, and then decrease when the KOH concentration further increases [28]. Yang *et al.* discovered that the current density of ORR for the air electrode in 8 M KOH solution is much greater than that of air electrode in 1 and 4 M KOH solutions [29].

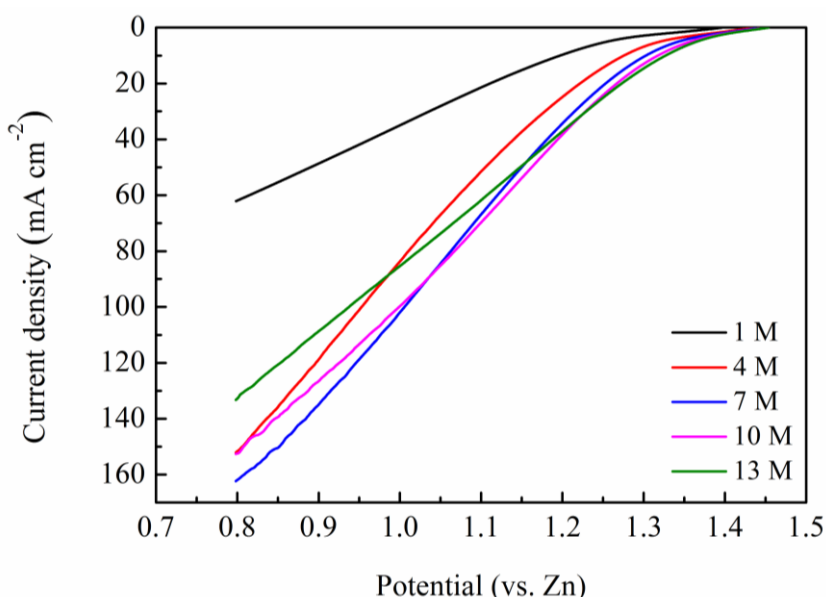
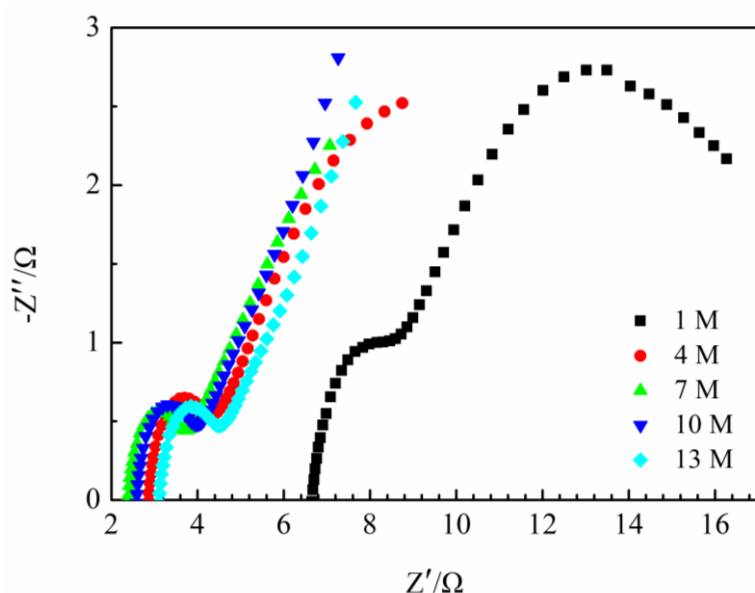


Figure 7. Polarization curves of ZAFCs with different electrolyte concentrations

Table 3. Performances of ZAFCs in difference KOH concentrations

	1 M	4 M	7 M	10 M	13 M
Current density at 1.0 V vs. Zn (mA cm^{-2})	35.0	83.8	102.0	99.8	85.4

Fig. 8 shows Nyquist plots of the same ZAFC in different KOH concentrations. Table 4 shows the calculated results from the simulated data of EIS in the ZAFC mode with the equivalent circuit shown in Fig. 3. As seen in Table 3, R first increased and then decreased when the KOH solution concentration increased, it is correlated with the electrolyte resistance in the ZAFC. R1 appears to decrease in accordance with the predicted increase of the KOH conductivity with concentration. R2 also increases with a increasing the KOH concentration in the low frequency semicircle. The effect has been obbtained by others [21].

**Figure 8.** Impedance measurements of ZAFCs with different electrolyte concentrations**Table 4.** Fitted partial data of equivalent circuit parameters about impedance spectra of ZAFCs in different KOH concentrations

	1 M	4 M	7 M	10 M	13 M
R	6.68	2.88	2.39	2.59	3.12
R1	1.56	1.28	1.02	0.99	0.96
R2	10.32	11.71	17.25	3.07E+3	4.46E+6

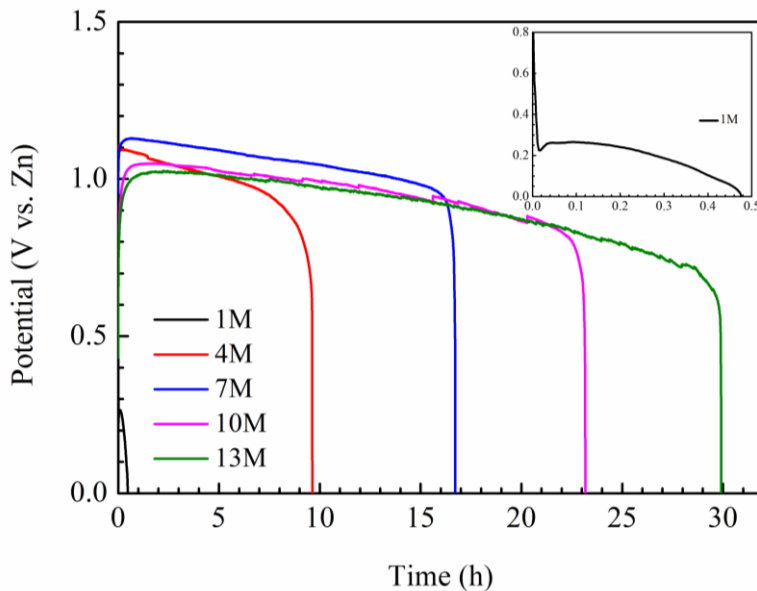


Figure 9. Discharge curves of ZAFCs operated in different KOH electrolyte

Fig. 9 shows discharge curves of ZAFCs operated in different KOH electrolyte. As seen in Table 5, the highest OCV of ZAFCs was obtained at 4 M. However, the peak value of the average operating voltages is 1.06 V (vs. Zn) at 7 M. The discharge time increase with increasing KOH concentrations from 1 M to 13 M. The average operating voltages for 0.2, 0.4 and 0.6 M KOH electrolytes were 1.10, 1.01 and 0.97 V, respectively. And, the batteries exhibited a marked decrease of discharge capacity with the inclusion of 0.2 and 0.4 M KOH in the agar; the capacity of the batteries was 477.5 and 392.5 mA h g^{-1} , respectively. The battery that contained agar with 0.6 M KOH battery showed the lowest discharge capacity, which was 272.5 mA h g^{-1} [30]. Average working voltage of Zn/MCM-41/air cell in 3 and 6 M KOH solution is 1.24 and 1.20 V at 5 mA cm^{-2} , respectively [16].

Table 5. Performance parameters of ZAFCs in difference KOH concentrations

	1 M	4 M	7 M	10 M	13 M
Open circuit voltage (V)	0.86	1.07	0.99	0.54	0.49
Average working voltage (V)	0.22	1.01	1.06	0.98	0.94
Discharge time (h)	0.5	9.6	16.7	23.2	29.9

3.3 Effect of the depth of discharge for ZAFCs

Fig. 10 shows polarization curves of ZAFCs with different discharge time. From this figure and Table 6, single cell current density decrease is attributed to the increase discharge time. The observed trend is favorable for confirming the time of replacing the zinc plate and (or) the electrolyte. Effect of discharge currents on ZnO synthesized by the zinc-air system was reported [31]. On the contrary, with the increase of current density discharge time reduced.

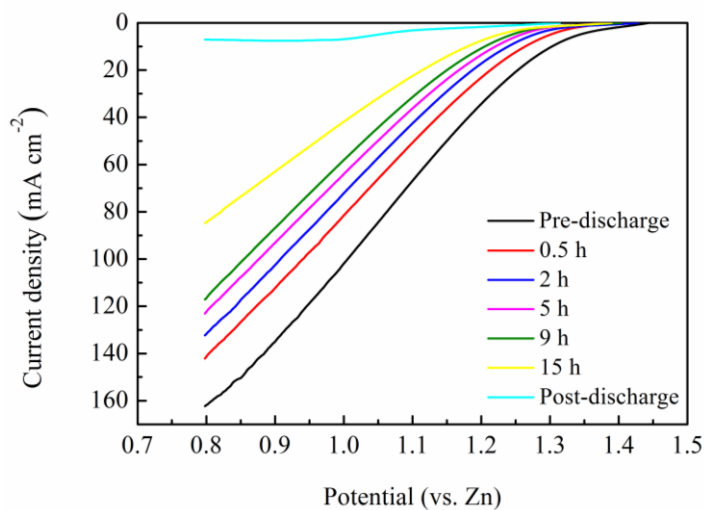


Figure 10. Polarization curves of ZAFCs with different discharge time

Table 6. Performances of ZAFCs with difference discharge time

	Pre-discharge	0.5 h	2 h	5 h	9 h	15 h	Post-discharge
Current density at 1.0 V vs. Zn (mA cm ⁻²)	102.0	81.6	72.2	64.0	58.1	41.9	6.9

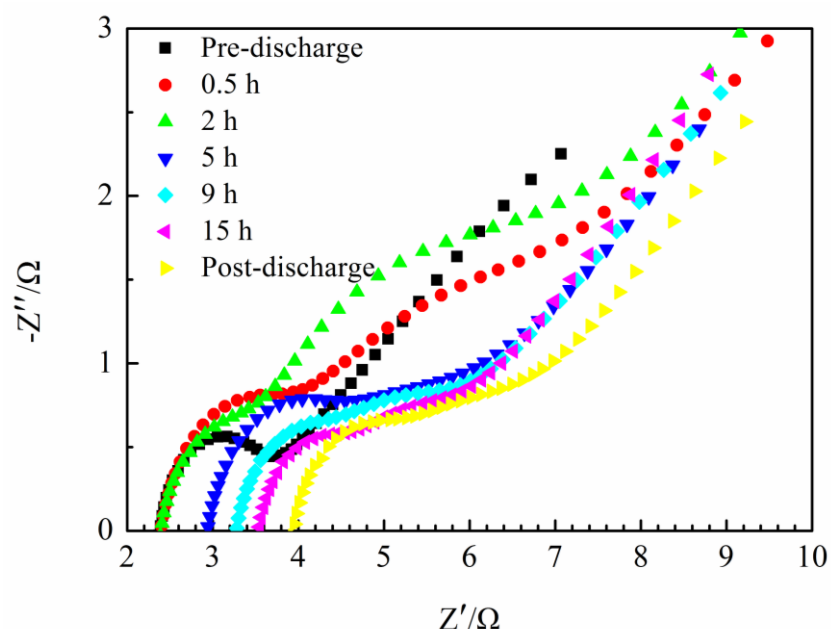


Figure 11. Impedance measurements of ZAFCs with different discharge time

Fig. 11 shows impedance spectra of the same ZAFC in different discharge time. Table 7 shows the parameters evaluated from the simulated data of EIS in the ZAFC mode with the equivalent circuit shown in Fig. 3 by ZView. As seen in Table 4, some trends can be obtained with respect to the difference resistances of the equivalent circuit. R decreased in high-frequency when the discharge time increased, it is related to total ohmic resistance in the ZAFC. R1 appers to wave, it is strongly related to the electrolyte conductivity. R2 decreased when the discharge time increased, which is expected since it is related to kinetics [20].

Table 7. Fitted partial data of equivalent circuit parameters about impedance spectra of ZAFCs with difference discharge time

	Pre-discharge	0.5 h	2 h	5 h	9 h	15 h	Post-discharge
R	2.39	2.40	2.41	2.94	3.28	3.54	3.96
R1	1.02	1.04	0.67	1.52	0.62	0.65	1.78
R2	17.25	2.78	3.28	1.43	1.29	1.17	1.11

4. CONCLUSION

In summary, a common ZnO of hexagonal nanorod structure was synthesized using a new method by the ZAFC. The experimental also study on the effect of the ZAFC was carried out for electrolyte concentration and depth of discharge by voltammetric, discharge profile and EIS methods. It is found that the concentration of electrolyte at 7 M, which was optimum for the ZAFC. Moreover, the performance of ZAFC decays with increasing discharge time. The observed trend is favorable for confirming the time of replacing the zinc plate and (or) the electrolyte in ZAFC.

ACKNOWLEDGEMENT

This work is partly supported by the Department of Science and Technology, Jiangsu Province (BY2013073-03), the Department of Education for the Fundamental Research Funds for the Central Universities, Jiangsu Province for the College graduate research and innovation projects (CXLX12_0105), and Analytical Test Fund of Southeast University (201226).

References

- 1 S.I. Smedley, X.G. Zhang, *Journal of Power Sources* 165 (2007) 897-904.
- 2 Y. Li, H. Dai, *Chemical Society reviews* 43 (2014) 5257-5275.
- 3 M. Armand, J.-M. Tarascon, *Nature* 451 (2008) 652-657.
- 4 P. Pei, K. Wang, Z. Ma, *Applied Energy* 128 (2014) 315-324.
- 5 J.S. Lee, S. Tai Kim, R.G. Cao, N.S. Choi, M.L. Liu, K.T. Lee, J. Cho, *Advanced Energy Materials* 1 (2011) 34-50.
- 6 K. Harting, U. Kunz, T. Turek, *Zeitschrift für Physikalische Chemie* 226 (2012) 151-166.

- 7 N. Alias, A.A. Mohamad, *Journal of King Saud University-Engineering Sciences* (2013) doi:org/10.1016/j.jksues.2013.1003.1003.
- 8 V. Neburchilov, H.J. Wang, J.J. Martin, W. Qu, *Journal of Power Sources* 195 (2010) 1271-1291.
- 9 P. Pei, Z. Ma, K. Wang, X. Wang, M. Song, H. Xu, *Journal of Power Sources* 249 (2014) 13-20.
- 10 P. Sapkota, H. Kim, *Journal of Industrial and Engineering Chemistry* 15 (2009) 445-450.
- 11 G.M. Wu, S.J. Lin, C.C. Yang, *Journal of Membrane Science* 280 (2006) 802-808.
- 12 A. Puapattanakul, S. Therdthianwong, A. Therdthianwong, N. Wongyao, *Energy Procedia* 34 (2013) 173-180.
- 13 W.-K. Chao, C.-M. Lee, S.-Y. Shieu, C.-C. Chou, F.-S. Shieu, *Journal of Power Sources* 177 (2008) 637-642.
- 14 M.N. Masri, M.F.M. Nazeri, C.Y. Ng, A.A. Mohamad, *Journal of King Saud University - Engineering Sciences* (2013) doi:org/10.1016/j.jksues.2013.1006.1001.
- 15 Y.-D. Cho, G.T.-K. Fey, *Journal of Power Sources* 184 (2008) 610-616.
- 16 H. Saputra, R. Othman, A.G.E. Sutjipto, R. Muhida, *Journal of Membrane Science* 367 (2011) 152-157.
- 17 H.S. Kim, Y.N. Jo, W.J. Lee, K.J. Kim, C.W. Lee, *Electroanalysis* 27 (2015) 517-523.
- 18 A.L. Zhu, D. Duch, G.A. Roberts, S.X.X. Li, H. Wang, K. Duch, E. Bae, K.S. Jung, D. Wilkinson, S.A. Kulinich *ChemElectroChem* 2 (2015) 134-142.
- 19 Z.L. Wang, *Journal of Physics: Condensed Matter* 16 (2004) R829-R858.
- 20 F. Bidault, D.J.L. Brett, P.H. Middleton, N. Abson, N.P. Brandon, *International Journal of Hydrogen Energy* 35 (2010) 1783-1788.
- 21 S. Zhu, Z. Chen, B. Li, D. Higgins, H. Wang, H. Li, Z. Chen, *Electrochimica Acta* 56 (2011) 5080-5084.
- 22 F. Bidault, A. Kucernak, *Journal of Power Sources* 195 (2010) 2549-2556.
- 23 M. Prabu, P. Ramakrishnan, H. Nara, T. Momma, T. Osaka, S. Shanmugam, *ACS applied materials & interfaces* 6 (2014) 16545-16555.
- 24 G. Chen, H. Zhang, H. Ma, H. Zhong, *Electrochimica Acta* 54 (2009) 5454-5462.
- 25 C.-C. Hu, S.-C. Liao, K.-H. Chang, Y.-L. Yang, K.-M. Lin, *Journal of Power Sources* 195 (2010) 7259-7263.
- 26 D. Schröder, T. Arlt, U. Krewer, I. Manke, *Electrochemistry Communications* 40 (2014) 88-91.
- 27 C.K. Yap, W.C. Tan, S.S. Alias, A.A. Mohamad, *Journal of Alloys and Compounds* 484 (2009) 934-938.
- 28 Y.L. Cao, H.X. Yang, X.P. Ai, L.F. Xiao, J. *Electroanal. Chem.* 557 (2003) 127-134.
- 29 C. Yang, S. Hsu, W. Chien, M. Changshih, S. Chiu, K. Lee, C. Liwang, *International Journal of Hydrogen Energy* 31 (2006) 2076-2087.
- 30 M.N. Masri, A.A. Mohamad, *Corrosion Science* 51 (2009) 3025-3029.
- 31 W.C. Tan, A.A. Mohamad, *Journal of The Electrochemical Society* 157 (2010) E184.